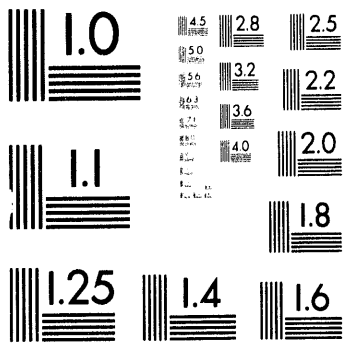
1.0
1.1
1.25
4.5
5.0
5.6
2.8
3.2
3.6
4.0
2.5
2.2
2.0
1.8
1.4
1.6

1 of 1

IS-M 772

DEVELOPMENT OF SMALL PUNCH TESTING TECHNIQUE AND ITS APPLICATION TO EVALUATION OF MECHANICAL PROPERTIES DEGRADATION

J. Kameda

Ames Laboratory
Iowa State University
Ames, IA 50011

Abstract

The present paper summarizes a small punch (SP) testing technique developed at Ames Laboratory and its application to mechanical properties characterization. It has been clearly shown on ferritic alloys that the SP test has capability to evaluate the intergranular embrittling potency of segregated solute, such as P, Sn and Sb causing temper embrittlement, and the effects of neutron irradiation and post-irradiation annealing, giving rise to changes in the hardness and intergranular solute segregation, on the fracture properties in terms of the ductile-brittle transition temperature (DBTT). A linear relationship of the DBTT determined by the SP test to that by Charpy V-notched tests has been theoretically and experimentally established. In Al alloy substrates coated with amorphous and overlaying ceramics, moreover, the global and local fracture properties were well characterized by the SP test together with acoustic emission techniques.

Introduction

The development of miniaturized testing methods is urgently required for evaluating the mechanical properties degradation in aging structural components (i.e., steam turbines and nuclear or fossil pressure vessels) and candidate materials for future fusion reactors, and the local mechanical properties in coated materials because of several following reasons [1,2].

(1) Conventional testing specimens like Charpy V-notched (CVN) specimens are too large to be extracted from aging structural components without causing mechanical damage during sampling.
(2) Small radioactive samples can be readily handled.
(3) The space of neutron irradiation facilities is very limited.
(4) Standard mechanical testing methods are not sensitive enough to characterize the near surface properties of coated materials.

A small punch (SP) testing technique has been developed at Ames Laboratory and its application has been successively made to examine the degree of temper and radiation embrittlement, and the post-irradiation annealing (PIA) effect with a special emphasis on grain boundary weakening [3-7]. The deformation and fracture behavior of coated materials has been recently studied using the SP test together with acoustic emission (AE) techniques [8]. This paper attempts to review our research efforts.

Small Punch Testing Technique

The materials presented in this paper were various model ferritic alloys (Ni-Cr steels and Fe base alloys) doped with controlled amounts of various metalloid impurities (P, Sn and Sb) and 7075 Al alloy substrates coated with Ni-10 wt.% P amorphous and Y_2O_3 stabilized ZrO_2 ceramics. The chemical compositions and heat treatments of the ferritic alloys along with the mechanical properties obtained using conventional testing methods, and the coating processing condition are presented elsewhere [6,8-11].

SP specimens with the dimension of 10 mm x 10 mm x 0.5 mm were prepared from the undamaged portion of broken CVN specimens of the Ni-Cr steels and the heat treated Fe alloys. Subsized SP (SSP) specimens with the dimension of 4 mm diameter and 0.5 mm thick were made by punching the undamaged corner section of previously tested SP specimens. The coating surface had been covered with masking tapes in order to minimize the damage before the Al alloy substrate was mill-machined. The surface of SP and SSP specimens except the coating surface was mechanically polished using 600 grid emery papers.

The puncher and specimen holder designed for SP and SSP tests are illustrated in Fig. 1 [3,4]. The SP and SSP testing holders consist of an upper and lower die with a square and round groove, respectively, and four clamping screws. When the SP and SSP specimens were set, a slight clearance between the

bottom surface of the upper die and the top surface of the specimen was provided to maintain a stress-free state prior to loading. The coated SP specimen was placed so that the coating surface is subjected to the applied tensile stress. This clamping holder is capable of preventing specimens from cupping upward during punching and therefore the deformation was intensified in the region below the puncher. The bore diameter of the lower die was designed in order for the deformed specimens not to be subjected to frictional forces arising from the contact of the specimens with the inner wall of the lower die hole.

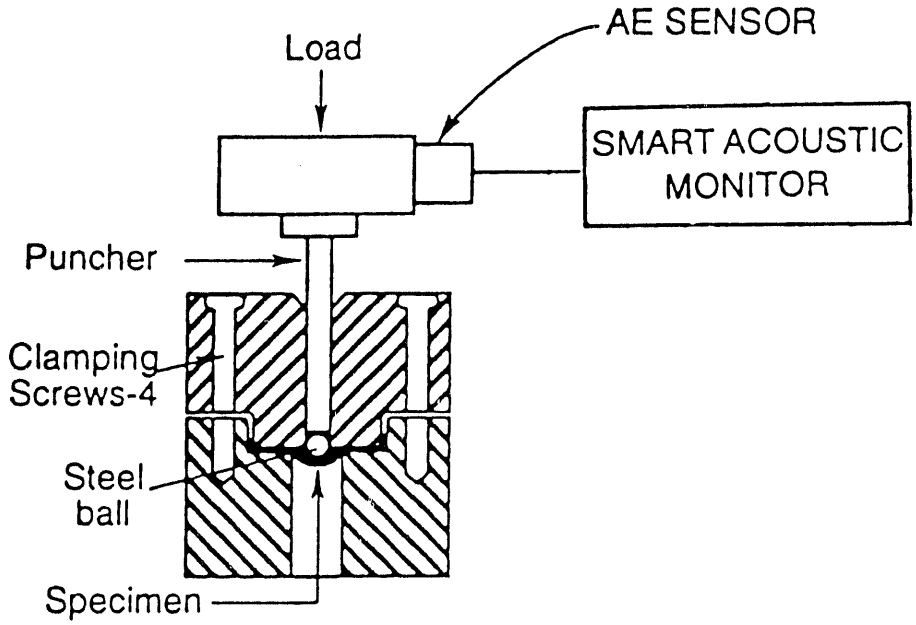

Figure 1 - Loading and specimen support configurations of small punch (SP) tests and attachment of acoustic emission (AE) sensor.

SP and SSP tests were carried out over a wide temperature range (77-500K) by placing the specimen holder in a screw-driven Instron testing machine. The specimen deformation was achieved by pushing the puncher with a ball of 2.4 mm diameter and a hemispherical tip of 1.3 mm diameter against the SP and SSP specimens, respectively, using a crosshead speed of 2×10^{-5} m/s. During the SP test on the coated materials, as indicated in Fig. 1, AE events and energy counts were measured to identify the coating cracking behavior using a sensor attached into the puncher and a smart acoustic monitor of Physical Acoustic Co [8].

Characterization of Deformation and Fracture Behavior

As schematically shown in Fig. 2, a typical load vs. deflection (P vs. δ) can be divided into four deformation regimes: (I) elastic bending, (II) plastic bending, (III) membrane stretching and (IV) plastic instability. The regime III indicates special deformation behavior observed during the SP test where the load-bearing capacity is drastically increased

with increasing δ [4,12]. From the P vs. δ curve, several parameters, such as the yield load (P_y), the deflection to failure (δ_f) and the fracture energy (E_y) are determined to characterize the deformation and fracture properties of materials.

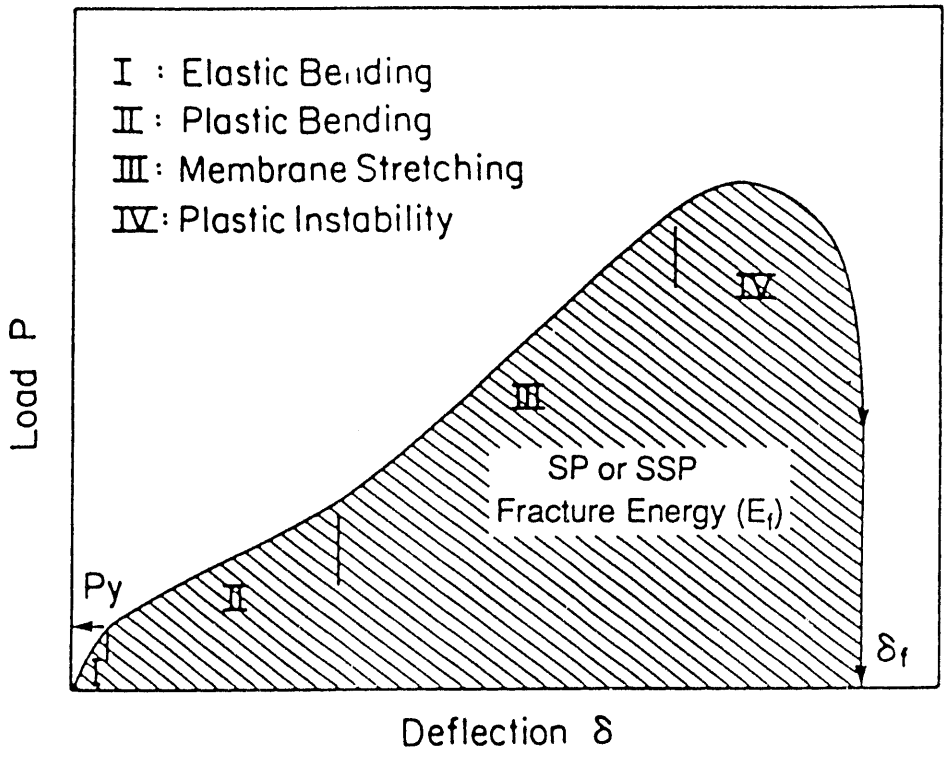

Figure 2 - Schematic illustration of load vs. deflection curve obtained from SP and SSP tests indicating four deformation regimes and several parameters representing the deformation and fracture properties.

Mao and Takahashi [13] have experimentally derived the relationship between P_y and the yield strength (σ_y) by performing the SP and tensile tests on several metallic materials with a wide variety of σ_y:

$$\sigma_y \text{ (MPa)} = 360(P_y/t_o^2) \text{ (KN/mm}^2\text{)} \quad (1)$$

where t_o is the initial specimen thickness. In order to analyze the ductile fracture behavior in the SP test, the radial strain distribution at the mid-section of load-interrupted and fractured SP specimens has been examined using a semi-analytical membrane stretching theory and a recrystallization etch technique [14]. It has been shown that ductile fracture usually occurs in the region along a circular plane inclined from the loading axis by about 45 degree solid angle where the equivalent plastic strain, which equals the thickness strain given by $\ln(t_o/t)$, is highly intensified. Because the thickness measurement in the axisymmetrically deformed SP specimens and the use of the recrystallization etch

method are impractical, the empirical relationship of ε_f to δ_f has been established [13-15]:

$$\varepsilon_f = 0.12(\delta_f/t_o)^{1.72} \quad \varepsilon_f > 0.05 \tag{2}$$

The estimated value of ε_f was found to be independent of the initial thickness and type of specimens.

The fracture toughness (J_{Ic}) represents the resistance of materials to ductile cracking which is an important parameter for engineering structural assessment while ε_f provides a relative measure of the material ductility. However, the J_{Ic} measurement requires the use of large specimens which is not appropriate to evaluate the mechanical properties degradation in aged or irradiated structural materials. Mao and Takahashi [13] have developed the correlation of J_{Ic} with ε_f based on fracture mechanics experiments in several materials with a wide range of the toughness together with an elastic-plastic analysis by Bayoumi and Bassim [16] as follows.

$$J_{Ic} = 345\ \varepsilon_f - 113 \quad (KJ/m^2) \quad \varepsilon_f > 0.4 \tag{3}$$

The DBTT has been widely used to investigate the degree of embrittlement of ferritic alloys. The SP and SSP tests clearly demonstrated the DBTT behavior in the plot of E_f against the temperature indicating the lower and upper shelf E_f [3,4,7]. In the lower shelf E_f, brittle cracks propagated along the radial direction unlike the ductile cracking morphology mentioned above. The E_f transition was found to occur more precipitously in the SP test than in the CVN test. This is because the ductile-brittle transition mode fracture takes place in the membrane stretching regime (III) where the load-carrying capacity rapidly increases (Fig. 2). The DBTT value can be defined by the temperature indicating the average value of the lower and upper shelf E_f.

The $(DBTT)_{SP}$ was observed in a substantially lower temperature range than the $(DBTT)_{CVN}$ [3,4]. The major cause for the difference in the DBTTs is that SP specimens are deformed under static loading and in a biaxial stress state which are mechanically less favorable for the occurrence of brittle cracking as compared with the dynamic test on CVN specimens containing the triaxial stress state. In order to establish a correlation between the $(DBTT)_{SP}$ and $(DBTT)_{CVN}$, a kinetic theory for the DBTT behavior has been developed [17]. In this theory, it is assumed that in the DBTT range ductile and brittle fracture can be characterized in terms of the thermally activated crack growth in shear and tension, respectively. Thus the fracture probability is represented by the product of the bond-breaking rate, the process volume (V) and the density of crack nuclei (F). The dislocation behavior which affects the local stress ahead of the crack tip is considered to be thermally activated under the applied strain rate($\dot{\varepsilon}$). At the DBTT, the ductile and brittle fracture probabilities become the same. Then the DBTT is described by the ratio of the thermal activation energy term representing the bond-breaking and

dislocation behavior near the crack tip to the mechanical and microstructural factors (F, V and $\dot{\varepsilon}$). Since the intrinsic fracture and deformation properties (i.e., the activation energy term) are independent of the testing condition, the correlation between the $(DBTT)_{SP}$ and $(DBTT)_{CVN}$ testing methods can be given by

$$(DBTT)_{SP} = \{\ln[(V_sF_s/V_tF_t)(\dot{\varepsilon}_o/\dot{\varepsilon})^2]_{CVN} / \ln[(V_sF_s/V_tF_t)(\dot{\varepsilon}_o/\dot{\varepsilon})^2]_{SP}\} (DBTT)_{SP} = \alpha(DBTT)_{CVN} \quad (4)$$

where $\dot{\varepsilon}_o$ is the parameter related to the dynamic material properties, and the subscripts s and t indicate shear and tension.

The relationship between the DBTTs was experimentally determined for several Ni-Cr, Cr-Mo-V and HT-9 steels with various yield strength, grain sizes, and types and amounts of impurities (Fig. 3) [15,17]. Despite some data scattering due to microstructural variations, a linear correlation can be observed in accord with the prediction of the kinetic theory.

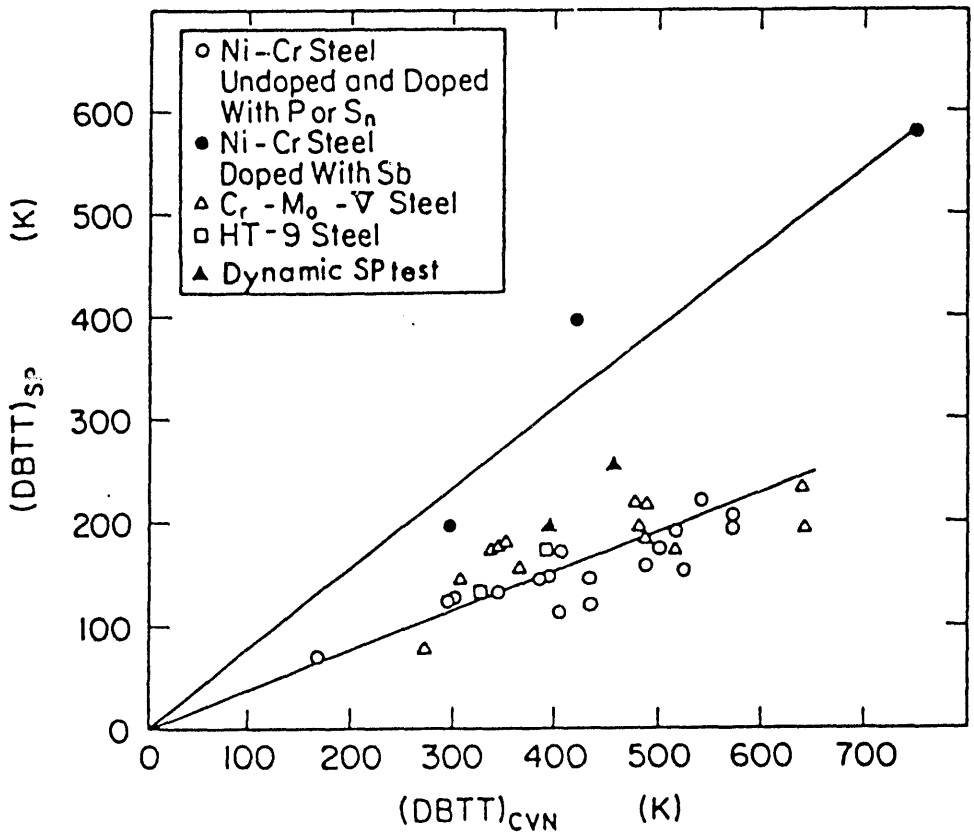

Figure 3 - Correlation between ductile-brittle transition temperature (DBTT) obtained from small punch (SP) and Charpy V-notched (CVN) tests for various ferritic alloy steels. The data of dynamic SP tests are also plotted.

The empirically determined value of α is about 0.4 for all the steels but a Sb-doped Ni-Cr steel. That is, the shift of the $(DBTT)_{CVN}$ becomes 2.5 times greater compared with that of the $(DBTT)_{SP}$. The data of dynamic SP tests by Joo, et al.[18] on two Cr-Mo-V turbine steels with different degree of embrittlement are also plotted using ▲ in Fig. 3. The dynamic SP results were found a little above the upper bound of the static ones. Therefore, it appears that the triaxial stress state plays a major role in determining the $(DBTT)_{CVN}$. Moreover, it is interesting to note [7,19] that the $(DBTT)_{SP}$ is not in good agreement with the DBTT determined by TEM disc specimen tests (the use of 1.0 mm punch tip, and 3 mm diameter and 0.25 mm thick specimens) but with the one obtained by the SSP. This suggests that the thickness of miniaturized testing specimens and the size of punch tips might controls the DBTT probably by affecting the process volume.

Temper Embrittlement

The fracture properties of ferritic structural alloys, which have been exposed to high temperatures (623-874°K) for a long period time, often are deteriorated due to temper embrittlement. The main causes of temper embrittlement are the intergranular segregation of embrittling solute like P, S, Sn and Sb and the evolution of carbide morphologies at grain boundaries which result in grain boundary weakening.

A fundamental study on solute segregation-induced intergranular embrittlement in model Ni-Cr steels individually doped with P, Sn or Sb, and having the same hardness and grain size has been made by performing four-point bend tests on notched bar specimens and tensile tests on precracked compact tension (CT) specimens in conjunction with selected area scanning Auger microscopy (SAM) analyses [9,10,20].

SAM analyses on the fracture surface have demonstrated that intergranular solute segregation has heterogeneous features related to the grain boundary structure and the distribution of alloying elements. The heterogeneous solute segregation produces different effects on the fracture properties depending on the type of specimens used. Using nonhomogenized and homogenized alloys with wide and narrow distributions of segregated Sb, it was found that the critical local tensile stress (σ^*) estimated from the notched bar test using a finite element stress analysis [21] and K_{Ic} determined from the precracked CT test represent the lowest and average fracture strength of grain boundaries embrittled by solute, respectively. The reason for this finding can be explained in the following. The formation of a brittle crack at the weakest grain boundary in a large highly stressed region ahead of the notch tip controls the specimen failure in terms of σ^*. On the other hand, the crack extension at many grain boundaries is required for the detectable cracking stage (K_{Ic}) in the precracked CT specimen because of the steeply distributed local stress. Figure 4 shows how the value of σ^* varies with the most probable maximum solute concentration at grain boundaries estimated using the Weibull extreme statistics and indicates the order of embrittling potency as follows: Sb > Sn > P.

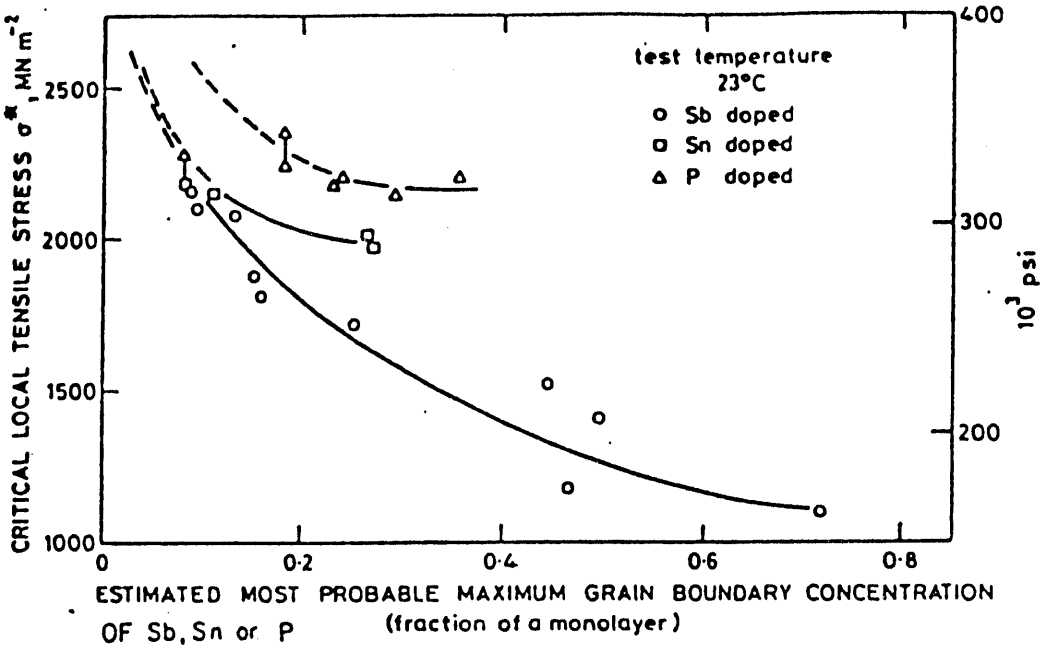

Figure 4 - Relationship of critical local tensile stress (σ^*) to most probable maximum grain boundary concentration of Sb, Sn or P.

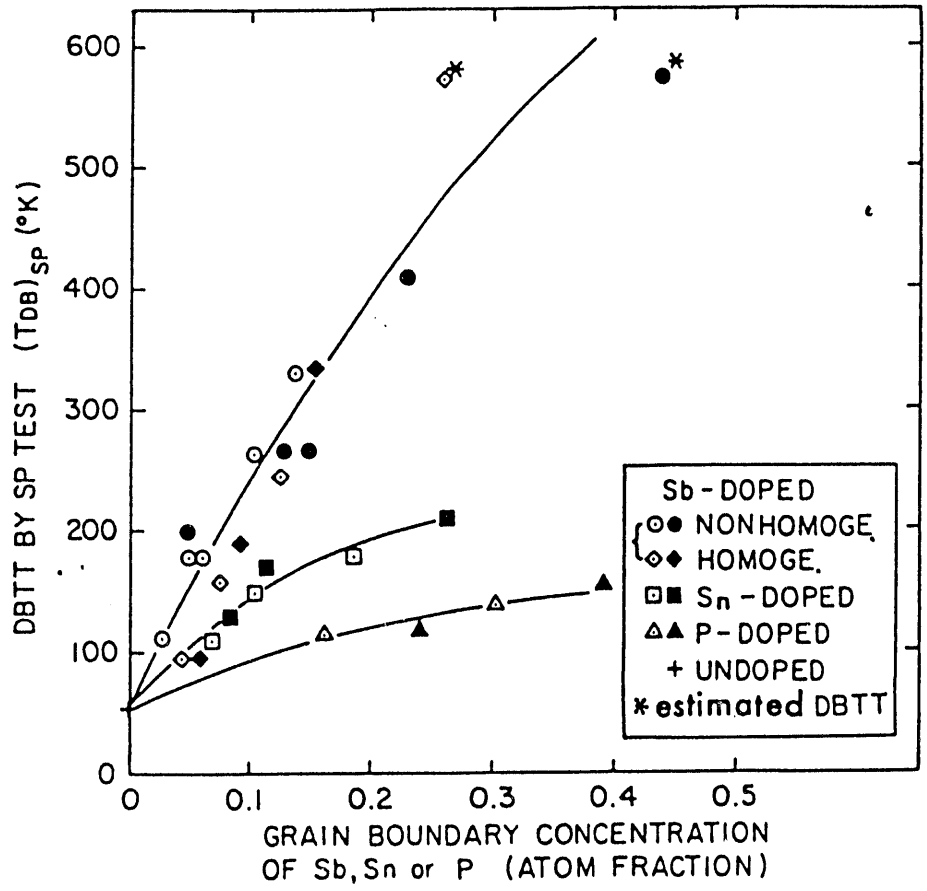

Figure 5 - Relationship of DBTT obtained from SP tests to concentration of segregated Sb, P and Sn indicating different embrittling potency. The lower and upper DBTT are plotted using open and closed points, respectively.

The SP test on the same embrittled steels was carried out in order to examine the relation to the aforementioned measurement of σ^* [5]. Serration was observed in the P vs. δ curve which is induced by discrete occurrence of intergranular cracks. Thus two types of E_f were defined at the initiation of serration and at peak load. The data of E_f were largely scattered in the DBTT range and the degree of the DBTT scattering increased with increasing heterogeneity of segregated solute and grain size [4,5]. The lower and upper DBTT values obtained from the SP test were plotted in Fig. 5 against the estimated maximum and average solute contents at grain boundaries, respectively. It is clear that the DBTT is uniquely correlated with the content of segregated solute independent of the nonhomogenized and homogenized alloys. By comparing Figs. 4 and 5, the embrittling tendency of various solute obtained from the SP test is consistent with the measurement of σ^*.

Radiation-Induced Embrittlement

It is well recognized in ferritic alloys that neutron irradiation produces the formation of very fine Cu and/or P rich precipitates and defect clusters in the grain matrix. Moreover, intergranular solute segregation is facilitated during high temperature neutron irradiation because of the dynamic interaction between solute and defect fluxes near grain boundaries. It is possible that hardening and intergranular segregation of embrittling solute induced by neutron irradiation results in a shift of the DBTT to high temperatures by reducing the dislocation mobility and grain boundary cohesion.

The effects of neutron irradiation (9.4×10^{22} n/m^2: E > 0.1 MeV at 668K) and PIA (623-873K for 0.1-1000 h) on the mechanical properties and grain boundary solute segregation have been investigated in various Fe alloys doped with Cu, P and/or C and containing residual S using the SP testing method, Vickers indentation tests and SAM [6,7,22,23].

The temperature dependence of σ_y estimated from the SP test on unirradiated and irradiated specimens is shown in Fig. 6 [6]. Cu and/or P doped alloys exhibited a greater hardening effect compared with C containing alloys. By analyzing the temperature dependence of the σ_y difference between the irradiated and unirradiated alloys, it is concluded that the hardening effect is mainly attributable to the formation of Cu and/or P rich precipitates and partially to that of defect clusters during the irradiation. The PIA effect on the microhardness was also investigated in the Cu and/or P doped alloys [7]. Hardening and softening, which is probably related to the density change in Cu/P rich precipitates, were generally observed during low and high temperature PIA, respectively. A Cu and P doped alloy exhibited the strongest hardening and least softening effects among all the alloys.

The SAM results of the unirradiated, irradiated and PIA treated alloys are summarized in the following. All the variously treated alloys exhibited intergranular S segregation.

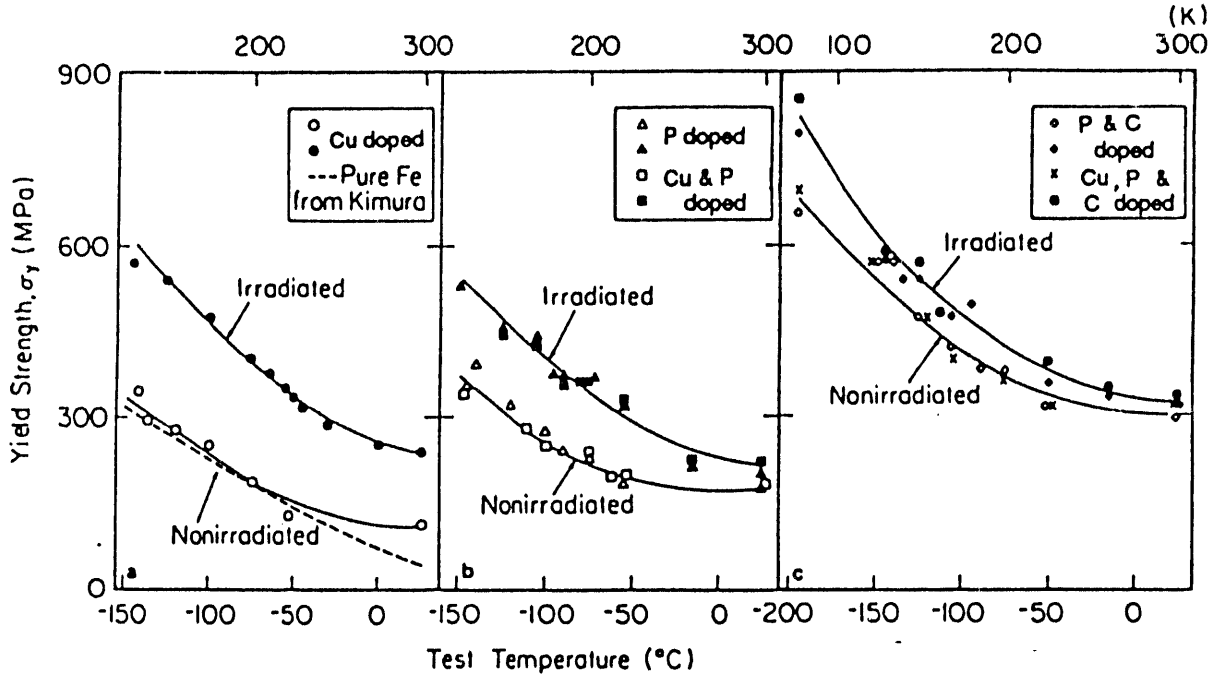

Figure 6 - Effect of neutron irradiation on yield strength (σ_y) estimated from SP tests in various Fe alloys.

Intergranular S segregation was increased by the neutron irradiation in a Cu doped alloy with negligible P segregation while it was decreased in P containing alloys due to the competitive segregation effect. In the Cu alloy, increasing the temperature and time of PIA promoted intergranular S segregation. The increasing rate of segregated S was much greater during the PIA compared with that observed in thermally annealed alloys. Intergranular P segregation was highly enhanced by the irradiation in the P containing alloys. The presence of Cu and C mitigated the irradiation effect on the P enrichment probably by interacting strongly with P and interstitials in the grain matrix. Intergranular P segregation was increased during an early stage of low temperature (623-688K) PIA. As the temperature and time of PIA were increased, intergranular P desegregation associated with an increase in S segregation dominated. Thus the critical temperature and time were identified at which the transition from P segregation to desegregation occurs. The solute segregation and desegregation behavior affected by the neutron irradiation and PIA can be explained in light of the competition between enriching and depleting fluxes of solute assisted by interstitials and vacancies, respectively, although better understanding of the jump of solute and defects in the region adjacent to grain boundaries is further required for the quantitative analysis.

The neutron irradiation shifted the DBTT to a higher temperature only in the Cu doped alloy while the PIA treatment significantly increased the DBTT in all the alloys. In order to demonstrate the neutron irradiation and PIA effects on the DBTT shift, the $(DBTT)_{SSP}$ are plotted against the microhardness and intergranular S segregation in Figs. 7 and 8, respectively. Although there is a tendency for the DBTT to increase with

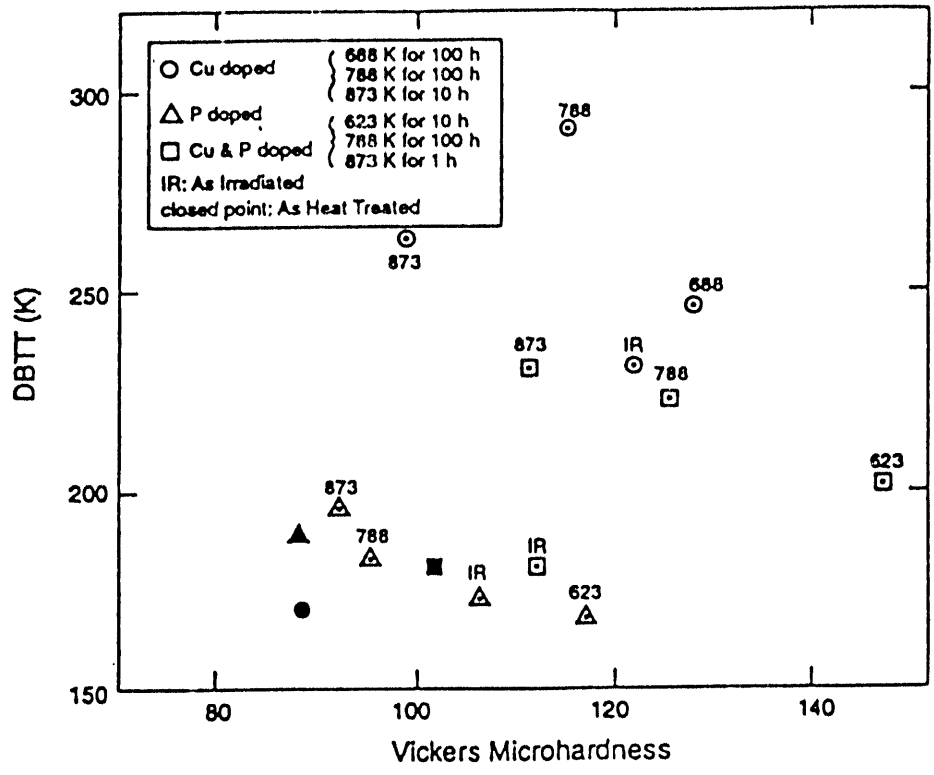

Figure 7 - Plot of DBTT obtained from SSP tests against microhardness for various unirradiated, irradiated and post-irradiation annealed Fe alloys.

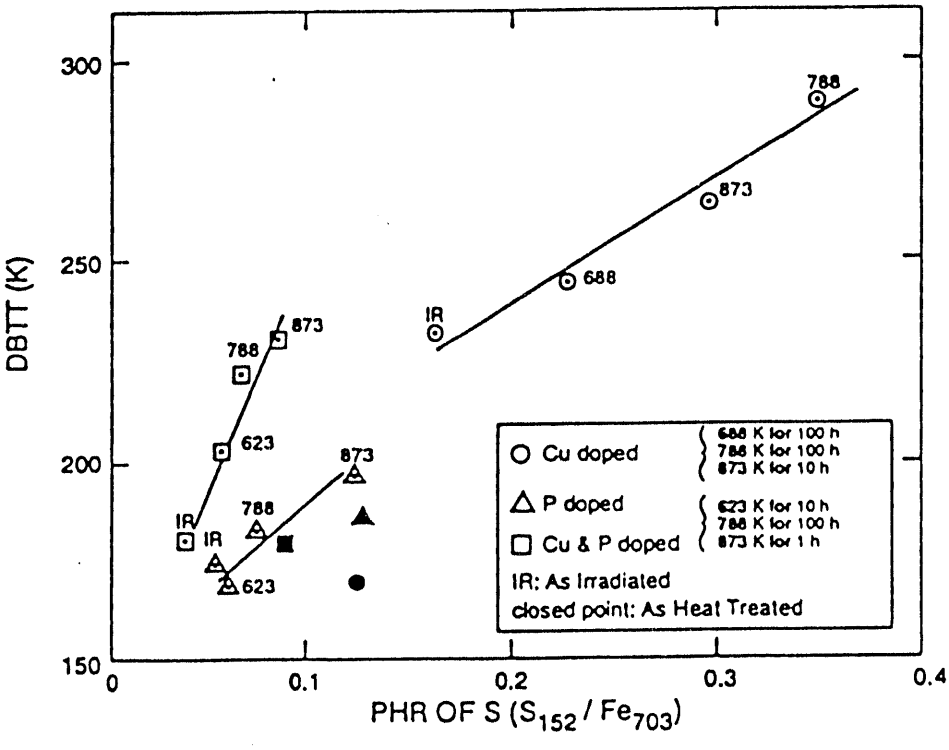

Figure 8 - Correlation of DBTT obtained from SSP tests with amount of segregated S for various unirradiated, irradiated and post-irradiation annealed Fe alloys.

increasing microhardness, a remarkable data scattering can be observed in Fig. 7. On the other hand, we can see linear correlations between the DBTT and amount of segregated S for all the irradiated and PIA treated alloys except the unirradiated ones (Fig. 8). In the Cu doped alloy with the absence of P segregation and small hardness changes, the S segregation effect predominantly controls the DBTT shift. The Cu and P doped alloy showed the strongest dependence of the DBTT on the S segregation because of the strong hardening effect induced by the PIA. In the P containing alloys, large amounts of P segregation were found not to affect the DBTT for the following reasons: (1) The P segregation is inversely related to the S segregated, and (2) the embrittling potency of P becomes much less compared with that of S particularly when the quantity of P is greater than 0.2 coverage.

Evaluation of Coated Materials

Because of the recent advancement of coating techniques, a variety of coating materials with excellent physical/chemical properties can be deposited on substrate materials and thereby the performance of structural and electrical materials can be drastically enhanced. Coated materials for structural and electrical applications are subjected to mechanical and/or thermal stresses. Therefore, there is a need to evaluate the mechanical properties of coated materials. However, the application of conventional testing methods is not useful for characterizing the local deformation and fracture behavior of coated materials.

An attempt has been made lately to examine the mechanical properties in Al alloy substrates coated with and without Ni-P amorphous (10 μm thick) and overlaying Y_2O_3 stabilized ZrO_2 (0-1.0 μm) ceramics by the SP testing and AE techniques [8]. The Al alloys coated with Ni-P and overlaying (0, 0.25, 0.5 and 1.0 μm thick) ceramics are designated as NP, NPZ1, NPZ2 and NPZ3, respectively.

Figure 9 shows the variation of σ_y, ε_f and J_{Ic} determined from the SP test as a function of coating, compared with the result of an uncoated alloy. The NP coating treatment gave rise to an increase in σ_y by 40% and increasing the thickness of overlaying ceramic coatings did not change σ_y. The fracture properties changed in a more complex manner depending on the type of coatings. The NPZ1 and NPZ3 coated alloys exhibited lower ε_f and J_{Ic} than the uncoated, and NP and NPZ2 coated ones. As shown in Fig. 10, many radial and tangential cracks were observed in the fractured SP specimens coated with Ni-P and/or overlaying ceramics.

The global fracture behavior of the coated alloys can be rationalized in light of the residual stress produced during the coating processing due to the thermal and elastic properties difference between the substrate and coating as well as stress concentration effects caused by the formation of coating cracks. The tensile residual stress on the coating surface, which is counterbalanced by the compressive and tensile stresses distributed below the coating/substrate

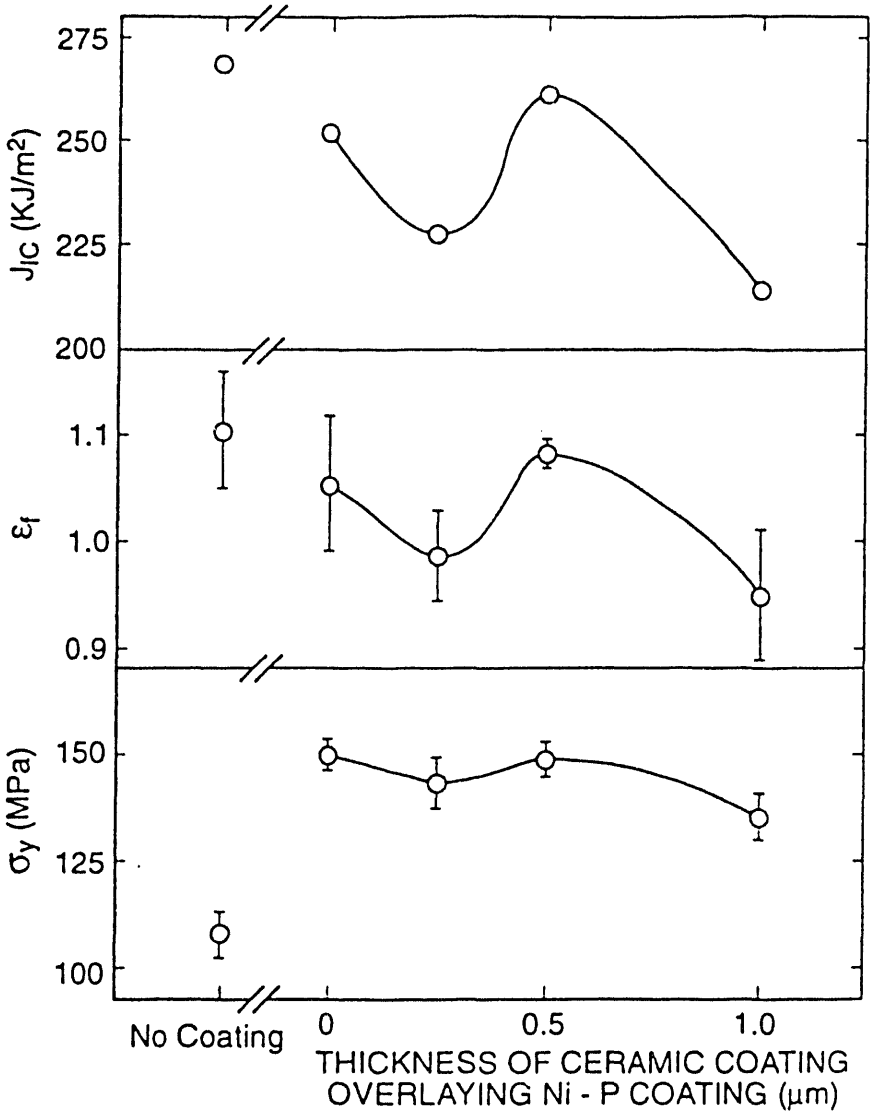

Figure 9 - Effect of various coatings on yield strength (σ_y), ductility (ε_f) and fracture toughness (J_{Ic}) estimated from SP tests.

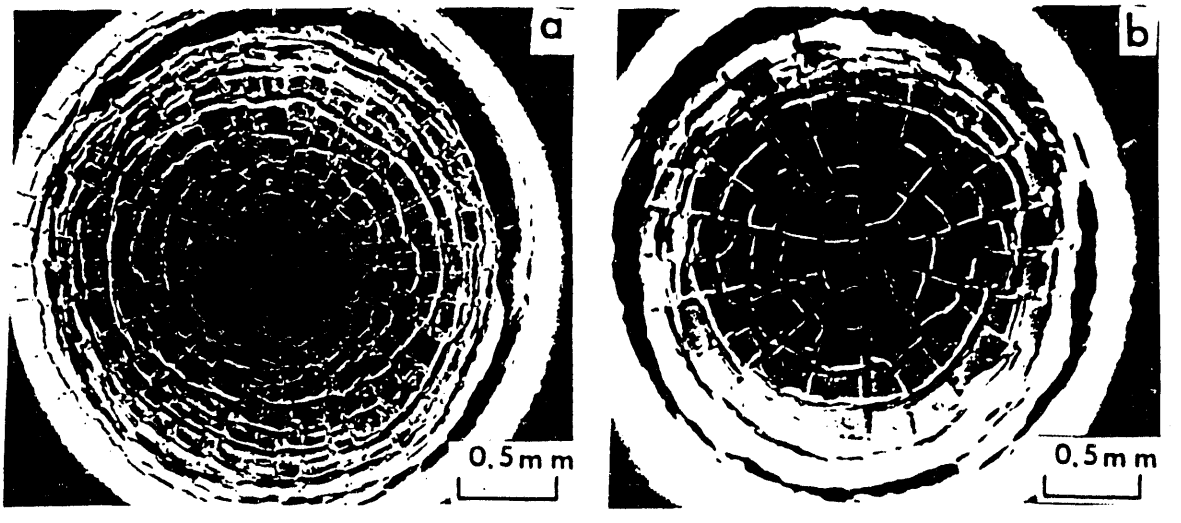

Figure 10 - Scanning electron micrographs of fractured SP specimens (a) coated with (a) Ni-P coating, and (b) Ni-P and overlaying (1.0 μm thick) ceramic coatings.

interface and near the substrate surface, respectively, was estimated using Stoney's formula [24]. It is clear from Fig. 11 that a much higher residual stress was observed in the NP and NPZ2 coatings than in the NPZ2 and NPZ3 coatings. In the NPZ1 and NPZ3 coated alloys having small residual stresses, the stress concentration effect caused by the coating cracks leads to a lowering of J_{Ic}. The value of J_{Ic}, which is relevant to the crack growth in the substrate, is probably more strongly controlled by the compressive residual stress below the interface than by the tensile one near the coating surface. Therefore, J_{Ic} in the NP and NPZ2 coated alloys is not much reduced by offsetting the stress concentration effect against the large compressive residual stress.

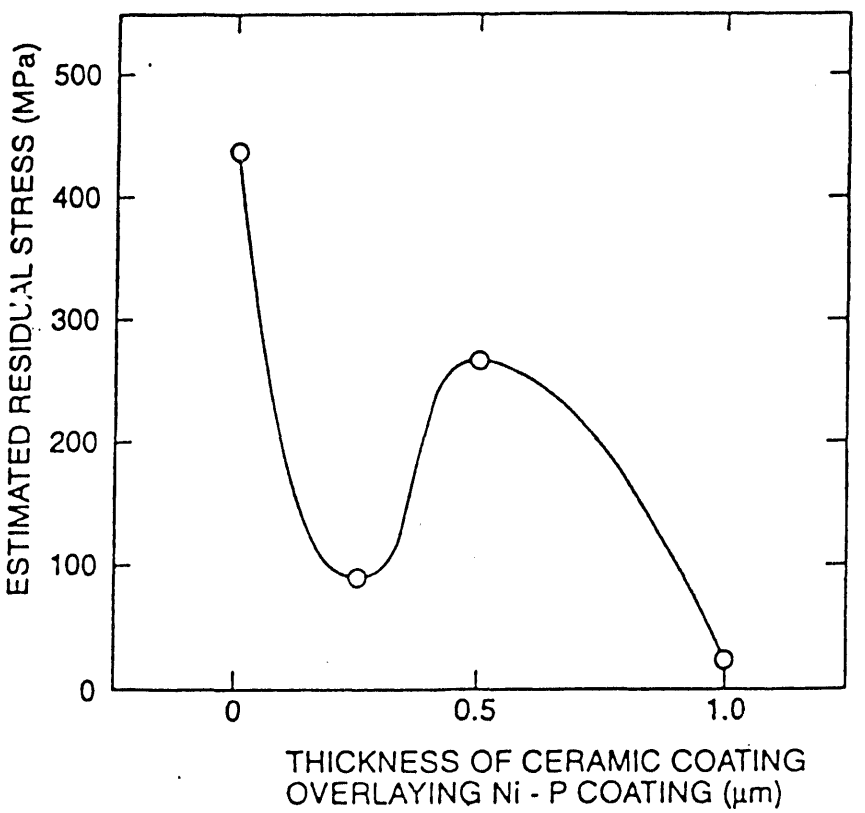

Figure 11 - Variation of estimated residual tensile stress as a function of various coatings.

The variation of the number of radial and tangential cracks, as well as fractured segments (N_r, N_t and N_s, respectively) with δ is indicated in Fig. 12. The NP coating showed a greater increasing rate of coating cracks in the plastic bending (II) and membrane stretching (III) regimes compared with the NPZ coatings. The density of coating cracks remained the same for all the NPZ coatings. The profound cracking behavior in the NP coating is attributed to the high tensile residual stress although the reason for observing no residual stress effects in the NPZ2 coating is not clear.

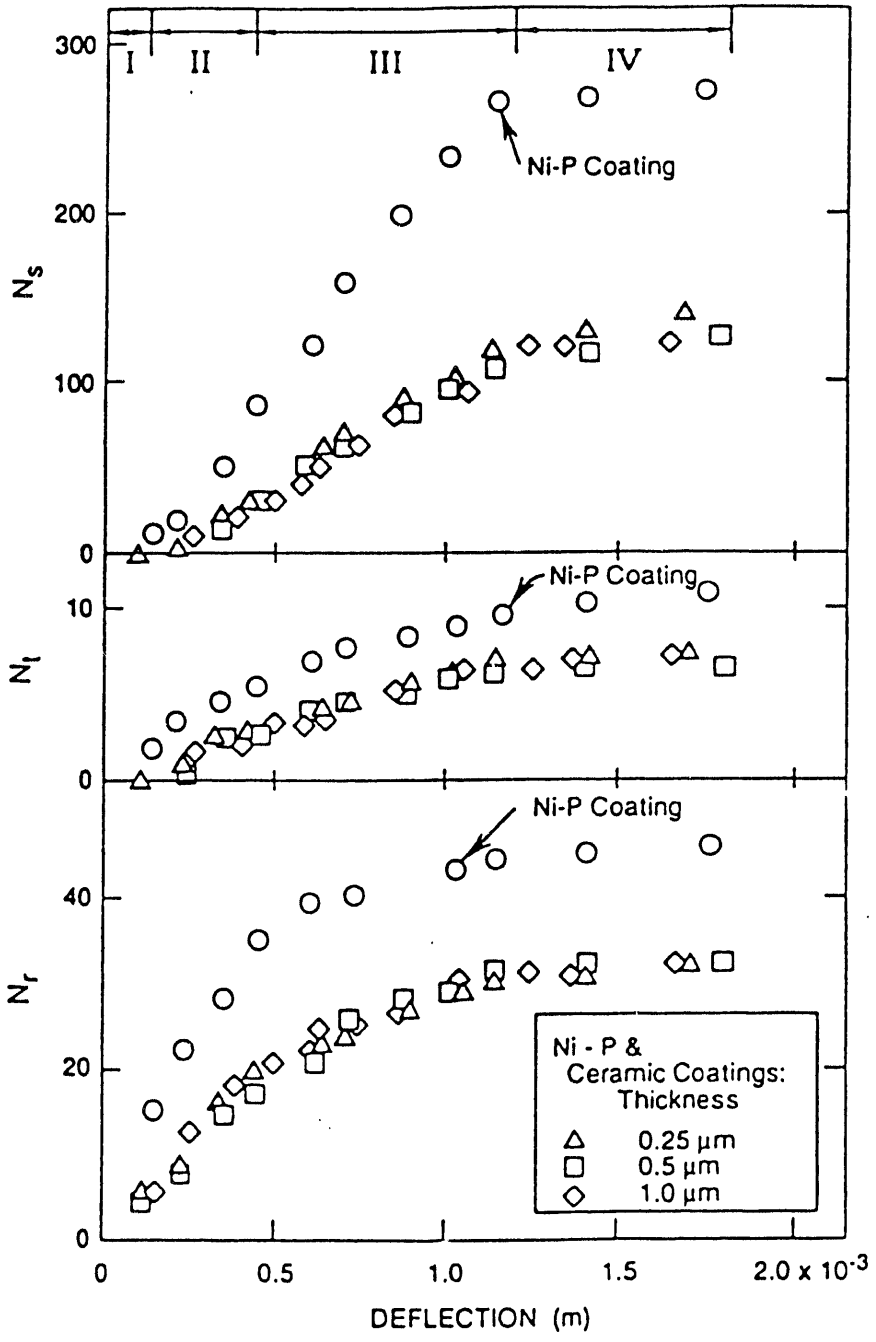

Figure 12 - Variation of numbers of radial and tangential cracks, and cracked segments (N_r, N_t and N_s, respectively) during deformation of coated SP specimens.

For the purpose of identifying nondestructively the coating cracking process, the AE activity was measured during the SP specimen deformation. Figure 13 delineates the relationship of N_r, N_t and N_s to the cumulative AE event for the various coatings. The coating cracking behavior is closely correlated with the AE event independent of the type of coatings within some data scattering band. It was also found that the intensity of individual AE events was increased with increasing the thickness of ceramic coating which is related to the propagation rate of the coating cracks.

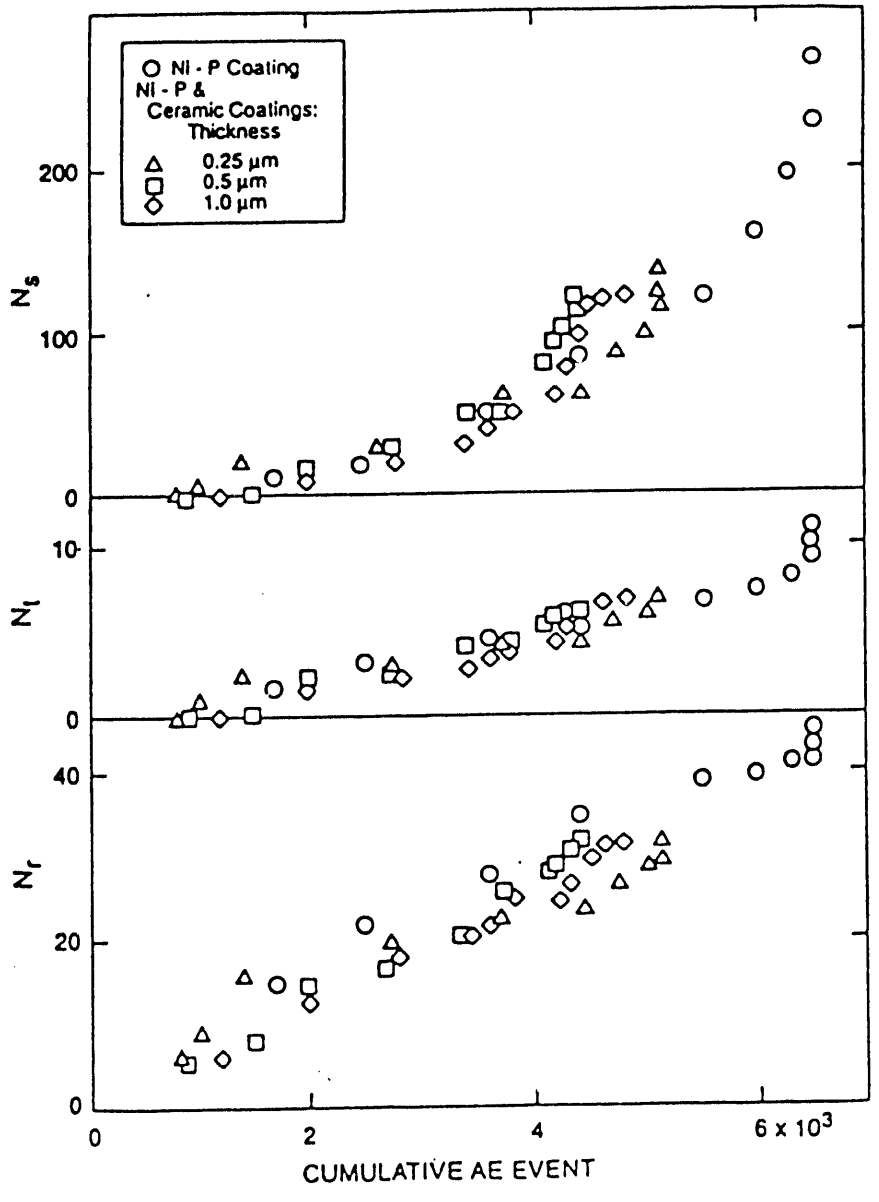

Figure 13 - Correlation of N_r, N_t and N_s with cumulative AE event during deformation of coated SP specimens.

From an engineering point of view, the initiation of coating cracks rather than the propagation becomes an important design criterion because once coating cracks are formed, the corrosion and wear resistance is dramatically decrease. Thus the detection of coating crack initiation is essential. Based on the present result, the measurement of AE events is shown to have ability to detect an early stage of coating cracks during the SP specimen deformation. Moreover, it is evident that the application of the SP and AE techniques is very promising for evaluating the local mechanical properties degradation in gas turbine blades made of Ni base superalloy substrates and intermetallic coatings which occurs under a high temperature oxidation environment, and high applied and thermal stresses.

Summary

The recent progress on the development of a miniaturized SP testing method and its application to mechanical properties characterization is reviewed. It has been shown that the SP test is capable of evaluating the mechanical properties degradation of several model ferritic alloys and coated materials. An analysis of the deformation and fracture behavior obtained from the SP test is presented. A kinetic theory provides a linear correlation between the $(DBTT)_{SP}$ and $(DBTT)_{CVN}$ which is supported by the experimental observation. The embrittling potency of metalloid impurities, radiation embrittlement and PIA effect are clearly evaluated in terms of the $(DBTT)_{SP}$ in conjunction with grain boundary solute segregation analyses. The SP testing and AE techniques can characterize well the global and local mechanical behavior in amorphous and overlaying ceramic coated materials.

Acknowledgments

Ames Laboratory is operated for the US Department of Energy by Iowa State University under contract no. W-7405-ENG-82. This work was supported by the Office of Basic Energy Sciences, Division of Materials Sciences.

References

1. R. Viswanathan and B. S. Bruemmer, Trans. ASME, J. Eng. Mater. Tech., 107 (1985), 316.

2. G. E. Lucas, Metall. Trans. A, 21A (1990), 1105.

3. J. M. Baik, J. Kameda and O. Buck, Scripta Metall., 17 (1983), 1443.

4. J. M. Baik, J. Kameda and O. Buck, The Use of Small-Scale Specimens for Testing Irradiated Materials, STP 888, eds. W. R. Corwin and G. E. Lucas (Philadelphia, PA: ASTM, 1986), 92.

5. J. Kameda and O. Buck, Mater. Sci. Eng., 83 (1986), 29.

6. J. Kameda and X. Mao, Mater. Sci. Eng., A112 (1989), 143.

7. J. Kameda, C. R. Gold and T. E. Bloomer, Proc. Sixth Inter. Sym. on Environmental Degradation of Materials in Nuclear Power Systems-Water Reactors, ed. E. Simonen (Warrendale, PA: TMS, 1994), in press.

8. J. Kameda and R. Ranjan, Mater. Sci. Eng. A, in press.

9. J. Kameda and C. J. McMahon, Jr., Metall. Trans. A, 11A (1980), 91.

10. J. Kameda and C. J. McMahon, Jr., Metall. Trans. A, 12A (1981), 31.

11. S. Takayama, T. Ogura, S. Fu and C. J. McMahon, Jr., Metall. Trans. A, 11A (1980), 1513.

12. M. P. Manahan, A. S. Argon and O. K. Harling, J. Nucl. Mater., 103-104 (1981), 1545.

13. X. Mao and H. Takahashi, J. Nucl. Mater., 150 (1987), 42.

14. X. Mao, T. Shoji and H. Takahashi, J. Test. Eval., 15 (1987), 30

15. J. Kameda and X. Mao, J. Mater. Sci., 27 (1992), 983.

16. M. R. Bayoumi and M. N. Bassim, Int. J. Fract., 23 (1983), 71.

17. J. Kameda, Acta Metall., 34 (1986), 2391.

18. Y. H. Joo, T. Hashida and H. Takahashi, J. Test. Eval., 20 (1992), 6.

19. T. Misawa, T. Adachi, M. Saito and Y. Hamaguchi, J. Nucl. Mater., 150 (1987), 194.

20. J. Kameda, Metall. Trans. A, 12A (1981), 2039.

21. J. R. Griffiths and D. R. J. Owen, J. Mech. Phys. Solids, 19 (1971), 419.

22. J. Kameda and A. J. Bevolo, Acta Metall., 37 (1989), 3283.

23. J. Kameda, C. R. Gold and T. E. Bloomer, unpublished work at Ames Laboratory (1993).

24. G. G. Stoney, Proc. Royal Soc. London, A 82 (1909), 172.

DATE
FILMED
12/13/93
END